Trisomic rescue via allele-specific multiple chromosome cleavage using CRISPR-Cas9 in trisomy 21 cells

Ryotaro Hashizume [ID][a,b,*], Sachiko Wakita[a], Hirofumi Sawada [ID][c], Shin-ichiro Takebayashi [ID][d], Yasuji Kitabatake [ID][e], Yoshitaka Miyagawa [ID][f], Yoshifumi S Hirokawa[g], Hiroshi Imai [ID][b,h] and Hiroki Kurahashi [ID][i]

[a]Department of Pathology and Matrix Biology, Mie University Graduate School of Medicine, Tsu, Mie 514-8507, Japan
[b]Department of Genomic Medicine, Mie University Hospital, Tsu, Mie 514-8507, Japan
[c]Department of Pediatrics, Mie University Graduate School of Medicine, Tsu, Mie 514-8507, Japan
[d]Laboratory of Molecular and Cellular Biology, Graduate School of Bioresources, Mie University, Tsu, Mie 514-8507, Japan
[e]Department of Pediatrics, Graduate School of Medicine, Osaka University, Suita, Osaka 565-0871, Japan
[f]Department of Biochemistry and Molecular Biology, Nippon Medical School, Tokyo 113-8602, Japan
[g]Department of Oncologic Pathology, Mie University Graduate School of Medicine, Tsu, Mie 514-8507, Japan
[h]Pathology Division, Mie University Hospital, Tsu, Mie 514-8507, Japan
[i]Division of Molecular Genetics, Institute for Comprehensive Medical Science, Fujita Health University, Toyoake 470-1192, Japan
*To whom correspondence should be addressed. Email: hashizumer@med.mie-u.ac.jp
Edited By Jorge Busciglio

Abstract

Human trisomy 21, responsible for Down syndrome, is the most prevalent genetic cause of cognitive impairment and remains a key focus for prenatal and preimplantation diagnosis. However, research directed toward eliminating supernumerary chromosomes from trisomic cells is limited. The present study demonstrates that allele-specific multiple chromosome cleavage by clustered regularly interspaced palindromic repeats Cas9 can achieve trisomy rescue by eliminating the target chromosome from human trisomy 21 induced pluripotent stem cells and fibroblasts. Unlike previously reported allele-nonspecific strategies, we have developed a comprehensive allele-specific (AS) Cas9 target sequence extraction method that efficiently removes the target chromosome. The temporary knockdown of DNA damage response genes increases the chromosome loss rate, while chromosomal rescue reversibly restores gene signatures and ameliorates cellular phenotypes. Additionally, this strategy proves effective in differentiated, nondividing cells. We anticipate that an AS approach will lay the groundwork for more sophisticated medical interventions targeting trisomy 21.

Keywords: human trisomy 21, chromosome loss, CRISPR/Cas, allele specificity, chromosome cut, Down syndrome

Significance Statement

An extra copy of chromosome 21 was discovered as the cause of Down syndrome more than half a century ago; however, methods to effectively remove the extra chromosome from trisomic cells are lacking. Using a system to rescue human cells with trisomy 21, this study successfully demonstrates the efficient elimination of excess chromosomes using multiple allele-specific targeting. Although a nonchromosome-breaking elimination method is desirable, the findings of this study can be used to rescue somatic cells with trisomy.

Introduction

Down syndrome (DS) is a genetic disorder caused by the presence of an extra copy of human chromosome 21 (HSA21). It is the most common viable chromosomal abnormality, occurring in ~1 in 700 live births (1). Extensive research has been conducted to elucidate the clinical features (2), genetic causes (3), and cellular characteristics (4) of DS. These studies have been aided by the development of innovative animal models (5) and advancements in prenatal diagnostic techniques, such as preimplantation genetic testing for aneuploidy (6). Despite these significant strides, a relative paucity of research has addressed the fundamental cause of DS.

Specifically, strategies are required to eliminate the extra chromosome from trisomic cells.

The clustered regularly interspaced palindromic repeats (CRISPR)/Cas9 nuclease system has emerged as a powerful tool for genome editing, enabling the precise insertion, deletion, or mutation of short DNA sequences at specific genomic loci of interest, including the removal of megabase-sized regions (7). Recent advances have demonstrated the feasibility of utilizing the CRISPR/Cas9 system to eliminate entire chromosomes by inducing targeted cleavages at multiple sites across homologous chromosomes (8, 9). These developments have paved the way for

therapeutic interventions targeting aneuploidy syndromes, such as trisomy 21, that address the fundamental genetic cause of these disorders. However, allele-nonspecific (ANS) cleavages can induce targeted random chromosome loss, as all homologous chromosomes are potentially subject to cleavage. While most genes on HSA21 maintain functionality in each copy, a small subset exhibits parent-of-origin-dependent silencing. For instance, DS cellular adhesion molecule is a paternally expressed imprinted gene (10). Meanwhile, several genes on HSA21, such as superoxide dismutase type 1, mitochondrial ribosomal protein L39, and SON, exhibit differential expression between alleles of parental origin (11). Consequently, in the context of trisomy 21, careful consideration must be given to selecting which chromosome is targeted for removal. This ensures that the intervention is directed toward a specific chromosome among the three homologs to mitigate the risk of potential imprinting disorders.

Haplotype phasing is required to precisely target a single chromosome with the CRISPR/Cas system, as it enables the determination of colocalized alleles on the same chromosome. However, genotype data obtained from recent comprehensive and whole-genome sequencing (WGS) techniques are typically presented without phasing. To address this challenge, we developed a phasing method that utilizes the chromosome elimination technique (12). In this way, a Cas9 system was designed capable of cleaving allele-specific (AS)-targeted chromosomes at multiple locations. Furthermore, we assessed the efficiency of excess chromosome removal in trisomy 21-induced pluripotent stem (iPS) cells and fibroblasts, providing insights into the potential application of this approach in the context of DS.

Results
Selection of the target allele and ANS or scramble gRNAs

In our previous work, we generated a trisomy 21 iPS cell line derived from skin fibroblasts and three induced disomy iPS cell lines with different combinations of HSA21 (ΔP, ΔM1, and ΔM2) using the chromosome elimination technique (Figs. 1A and S1) (12). Considering the reported existence of genes on HSA21 sensitive to maternal origin (11), the P allele was excluded from the Cas9 target. Among the alleles of maternal origin, the M2 allele was randomly selected as the Cas9 target homolog. ANS × 24 and ANS × 49 (24 and 49 repeats at the q-subtelomeric region on HSA21, respectively) were identified in the WGS data set as ANS Cas9 recognition loci (9) in each HSA21 allele (ANS × 24: ΔP 379, ΔM1 443, and ΔM2 433 counted reads containing the consensus sequence, and ANS × 49: ΔP 399, ΔM1 440, and ΔM2 361 reads). Furthermore, reads containing the scramble guide RNA (gRNA) sequence and its reverse complement were confirmed to be absent from the WGS data sets for trisomy 21, ΔP, ΔM1, and ΔM2 cell lines, ensuring the specificity of the designed Cas9 system.

Selection of gRNA sequences based on DNA cleavage efficacy

To identify M2-specific Cas9 recognition sequences, all Cas9 recognition sequences were extracted from each of the four samples: original trisomy 21 and the induced disomy cell lines ΔP, ΔM1, and ΔM2. Subsequently, a set operation was performed on the data sets, identifying 15,695 Cas9 recognition sequences specific to the M2 allele. Among these, 7,697 (49.0%) candidates were located in the q-subtelomeric region, occupying only 10.7% of HSA21, followed by 4,283 (27.3%) and 3,428 (21.8%) in the q- and p-arms,

respectively (Fig. 1B). Fifty-six M2-subtelomere target sequences were selected based on the number of EGxxFPs plasmids (13), inserting the smallest possible genomic region for cleavage efficiency evaluation, with each target sequence located nearby. The 21 genomic fragments containing the gRNA target site (length: 257–1,509 bp, average 812 bp) were amplified using PCR and subcloned into the pCAG-EGxxFP reporter plasmid. One target site was not selected due to the presence of only off-target sequences obtained from 10 colonies. The remaining 55 target sites were evaluated for gene-targeted endonuclease activity of Cas9 coexpressed with gRNA plasmid vectors in the EGxxFP system. One target site exhibiting digestion activity independent of Cas9 was excluded. Of the remaining 54 sites, Cas9/gRNA cleaved only on-target DNA sequences, not off-target sequences, at 18 sites (33.3%), cleaved on- and off-targets at 31 sites (57.4%), and cleaved neither on- nor off-targets at 5 sites (9.3%). Notably, no pattern was observed in which Cas9/gRNA cleaved only off-target sequences (Fig. 1C and Table S1).

AS chromosome cuts induce chromosome loss in a cleavage site number-dependent manner

To investigate whether CRISPR/Cas9-mediated chromosome breaks can correct the karyotype of trisomy 21 cells, AS systems were developed that exclusively recognize sequences unique to a single HSA21 (M2) and ANS systems that recognize all three HSA21s (Fig. 2A and C). We generated Cas9–RNA(s) coexpression vectors that cut the M2 allele at sites 1–13 for AS cuts, and three ANS vectors were prepared (ANS × 24, ANS × 49, and ANS × 73). The M2 AS Cas9 recognition sequences were randomly selected from 18 sequences exhibiting M2 AS cleavage activity, as evaluated using the pCAG-EGxxFP reporter (Fig. 1C). These all-in-one Cas9–gRNA(s) vectors were electroporated into trisomy 21 iPS cells, and the karyotype correction rate was assessed using fluorescence in situ hybridization (FISH) with HSA21-specific probes (Fig. 2C). The number of cleavage sites and corresponding chromosome elimination rates (averages ± SD) were as follows: ×1 (1.0 ± 1.7%), ×2 (2.6 ± 1.1%), ×4 (6.7 ± 2.3%), ×6 (7.7 ± 1.5%), ×8 (7.8 ± 0.4%), ×10 (11.4 ± 1.6%), ×12 (11.3 ± 1.4%), and ×13 (13.1 ± 0.3%) (Fig. 2D). Haplotype-aware single or multiple chromosome cleavages successfully induced karyotype corrections. Since M2-specific double-stranded breaks (DSBs) with each gRNA showed no significant difference in chromosome elimination efficiency across the 13 sites (Fig. S2), the frequency of chromosome loss was proportional to the number of cuts introduced.

Repair gene inhibition enhances DSB-induced chromosome elimination frequency

The RNA-guided nuclease activity of Cas9 generates DSBs, which are the most detrimental to cells. In humans, three major pathways can repair DSBs: classical nonhomologous end joining (NHEJ), microhomology-mediated end joining (MMEJ), and homologous recombination. Although the pathway that repairs a particular DSB partially depends on the local DNA sequence, chromatin packaging, and cell cycle stage, NHEJ and MMEJ are the primary repair pathways following DSBs (13). To determine whether suppressing chromosomal DNA repair ability affects the elimination of chromosomes by DSBs, the DNA polymerase theta (POLQ) gene (encodes a key MMEJ protein (13)) and DNA ligase 4 (LIG4) gene (indispensable for NHEJ (14)) were simultaneously suppressed using small interfering RNA (siRNA) along with chromosome cleavage in iPS cells. Digital PCR validated the siRNA efficiency, with the knockdown persisting for 48 h post-
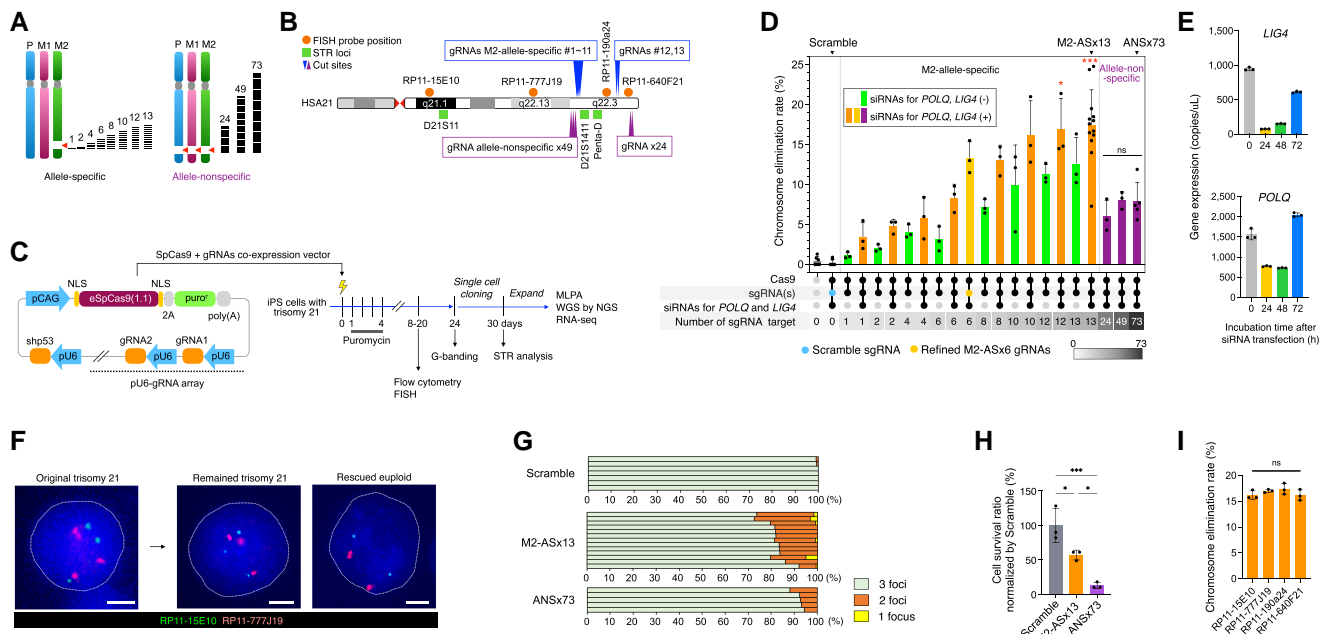
Fig. 1. Haplotype phasing strategy and validation of gRNA efficacy. A) Phasing of three copies of chromosome 21 in trisomy 21 cells. WGS data from four cell lines, including the original trisomy 21 and three induced disomy 21 cell lines wherein each chromosome 21 was deleted, were used to extract all SpCas9 recognition sequences. The set operation returned AS recognition sequences, enabling the phasing of the three copies of chromosome 21 in trisomy 21 cells. B) Plots representing the positions of 15,135 M2 AS Cas9 recognition loci in bins of 0.5 M bases on chromosome 21. C) Summary for validating 54 gRNA sequences to determine the efficacy of digesting the target sequence using the EGxxFP plasmids, an in vivo reporter system.

transfection (Fig. 2E). POLQ and LIG4 knockdown increased the rate of chromosome loss by an average of 1.78 times (range: 1.38-fold increase in ×13 to 2.67-fold increase in ×6) in all M2-specific allele cleavages from ×1 to ×13 (Fig. 2D). Representative FISH images of the original trisomy 21 iPS cells and cells after M2-specific allele cleavage ×13 + siRNA treatment (M2-AS × 13) and chromosomal components of the Scramble, M2-AS × 13, and ANS × 73 lines are shown in Fig. 2F and G, respectively.

AS targeting enhances chromosomal correction efficiency

To assess the efficacy of AS targeting compared with ANS targeting, chromosome breaks were induced at HSA21-specific repetitive sequences for ANS cleavages. Despite numerous cleavage sites, ANS cleavages exhibited a lower karyotype correction rate (6.0 ± 2.0%, 8.1 ± 1.1%, and 7.9 ± 2.4% for ANS × 24, ANS × 49, and ANS × 73, respectively) compared with AS cleavages. The AS cleavage groups, AS × 12 and AS × 13, exhibited statistically significant higher rates of chromosome elimination compared with all ANS cleavage groups (AS × 12: P < 0.05 and AS × 13: P < 0.0001 when compared with the three ANS groups). In ANS cleavage groups, no apparent correlation was found between the karyotype correction rate and the number of cleavage sites (Fig. 2D). The efficiency of plasmid transfer into trisomy iPS cells was 1.88 ± 0.47%, 1.07 ± 0.13%, and 0.24 ± 0.09% for the Scramble, AS (M2-AS × 13), and ANS (ANS × 73) cleavages, respectively. The cell survival rate after CRISPR/Cas9 treatment was considerably lower in the ANS × 73 (12.7 ± 4.6% when normalized to the Scramble) compared with that of the M2-AS × 13 (57.0 ± 7.1%) cleavage (Fig. 2H). These findings demonstrate that AS targeting is more efficient and less harmful to cells than ANS targeting for chromosomal correction.

DSBs induced by Cas9 divide a chromosome into two fragments with and without a centromere. If not repaired before mitotic entry, acentric fragments can be lost from the cell through micronucleus formation (15). Loss of acentric fragments results in chromosome truncation within the regions spanning the cut site to the telomere. As the chromosomal composition was evaluated

via FISH using a probe closer to the centromere than the cut sites, it was unclear how frequently terminal deletions of the q-arm developed following Cas9-mediated DSBs. To address this, the chromosome elimination rate was remeasured in the M2-AS × 13 sample using probes closer to the q-arm telomere, RP11-190a24, or RP11-640F21. No correlation was detected between the hybridization site of the probe and the chromosome elimination rate, suggesting that AS chromosome breaks in trisomic cells induce whole chromosome elimination rather than terminal deletion in most cells (Fig. 2I).

Next, to determine whether the targeted M2 chromosomes were lost chromosomes after CRISPR/Cas9-mediated chromosome cutting in trisomy 21 iPS cells, three-color reporter trisomy 21 cells were generated wherein the mTagBFP2-Neomycin resistance marker cistronic expression transgene was inserted into HSA21 at the HSF2BP intron 3 (21q22.3) of P allele, DsRed2-Puro was inserted into the M1 allele, and mEmerald-Hygro was inserted into the M2 allele (Fig. 3A). The loss of a specific fluorescence signaling indicated the loss of the allele into which the corresponding fluorescent sequence was inserted. The three-color reporter cells experienced spontaneous loss of fluorescence at a frequency of 17–25%, 10 days after antibiotic selection pressure was lifted, despite the absence of significant chromosome loss (Fig. S3). Thus, to exclude naturally nonfluorescent cells, considering that no monosomy or nullisomy of chromosome 21 was detected after M2-AS × 13 treatment by short tandem repeat (STR) analyses (Fig. 3D and E) and G-banding karyotyping (Fig. 4), cells with loss of only one fluorescent signal were counted and divided by the total cell number. In cells transfected with the Scramble, the P allele loss was 0.20% ± 0.10, M1 allele loss was 0.02 ± 0.01, and M2 allele loss was 0.04 ± 0.01. For the ANS × 73 vector, the corresponding ratios were 1.88 ± 0.89, 1.28 ± 0.64, and 2.88 ± 0.79, respectively, and for the M2-AS × 13 vector, they were 0.32 ± 0.10, 0.54 ± 0.14, and 7.17 ± 0.78, respectively (Fig. 3B and C). These results suggest that the M2-AS × 13 vector induces AS chromosome elimination, predominantly targeting the M2 allele.

Following transfection with the Scramble, ANS × 73, or M2-AS × 13 vectors, 72, 74, and 72 clones were established, respectively. All clones were subjected to STR analysis to determine their allele composition. In the transfection of the Scramble

Fig. 2. CRISPR/Cas9-mediated chromosome fragmentation and restoration of disomy in trisomic cells. A) Conceptual diagrams of AS and ANS chromosome cleavages. B) Location of chromosome breaks, FISH probes, and STR markers used in this study. The 21q22.3 region is drawn larger than its actual size for illustrative purposes. C) Plasmid map for all-in-one expression vectors to coexpress Cas9 and gRNA(s) and experimental scheme showing the introduction of the expression vectors into iPS cells with trisomy 21 and downstream analyses. pCAG, CAG promoter; NLS, nuclear localization signal; eSpCas9(1:1), S. pyogenes Cas9 variant with enhanced targeting specificity from Dr. Feng Zhang's lab; 2A, 2A peptide; puro^r, puromycin resistance gene; poly(A), polyadenylation signal; pU6, U6 RNA polymerase III promoter; shp53, short hairpin RNA against p53; FISH, fluorescence in situ hybridization; STR, short tandem repeat; MLPA, multiplex ligation-dependent probe amplification; WGS, whole-genome sequencing; NGS, next-generation sequencing. D) FISH analysis summary after transfection of various AS or ANS chromosome-breaking vectors ($n = 13$ for AS × 13, $n = 7$ for Scramble, $n = 5$ for ANS × 73, and $n = 3$ for other groups). The chromosome elimination rate (%) is the ratio of disomy 21 cells, determined using FISH, to the total number of cells into which the vector was introduced. The CN of chromosome 21 was determined via double-FISH using RP11-15E10 and RP11-777J19 probes. The numbers in the lower row represent the number of target sequences per allele. For ANS targets, the total number of targets per cell is three times the number indicated, as each allele contains the same target sequence. *$P < 0.05$ and ***$P < 0.0001$ compared with the three ANS groups. E) Validation of siRNAs for LIG4 and POLQ genes. F) Representative FISH images in interphase. Scale bars: 5 μm. G) Chromosomal components for the Scramble ($n = 7$), AS × 13 ($n = 13$), and ANS × 73 ($n = 5$) conditions. Each bar represents an independent test, and the percentage of cells exhibiting each chromosomal complement is based on the analysis of 102–215 cells per line. The total number of cells assessed for each condition was as follows: Scramble, 950; M2-AS × 13, 1,829; ANS × 73, 576. Abbreviations are as follows: M2-AS × 13, M2 allele-specific DSB × 13 with siRNAs; ANS × 73, allele-nonspecific DSB × 73 with siRNAs. H) Cell survival ratio for the Scramble, M2-AS × 13, and ANS × 73 vector transfection into trisomy 21 iPS cells, normalized by the Scramble data set. *$P < 0.05$, ***$P < 0.001$. I) Remeasurement of chromosome elimination rate in the M2-AS × 13 sample using probes closer to the q-arm telomere, RP11-190a24, or RP11-640F21. Data are represented as the mean ± SD.

vector, all clones showed trisomy 21, whereas disomy 21 appeared in five cells (6.8%) in the ANS × 73 lines and 22 cells (30.6%) in the M2-AS × 13 lines. Furthermore, the ANS × 73 lines had two (2.7%) delta-P disomy, one (1.4%) delta-M1, and two (2.7%) delta-M2 disomy, whereas the M2-AS × 13 lines had all delta-M2 in 22 disomy 21 cells. These findings reaffirm the ability of the M2-AS × 13 vector to induce targeted, AS chromosome loss and demonstrate its high efficacy in correcting the karyotype of trisomy 21 cells (Fig. 3D and E).

Chromosome breaks show no noticeable structural abnormalities in microscopically karyotyping

To assess the overall karyotype of cells after M2-AS × 13 vector transfection, the karyotypes were evaluated by G-banding 24 days after transfection. While the original trisomy 21 iPS cells showed a uniform 47,XY,+21 karyotype in all 19 metaphases (Fig. 4A), transfected cells exhibited a mix of 47,XY,+21 (62.5%) and 46,XY (37.5%) karyotypes in 40 metaphases (Fig. 4B). Microscopic examination within the high-resolution (band level: 400–550) G-banded karyotyping range revealed no detectable structural variants or other chromosomal numerical abnormalities.

Multiple cleavage events lead to diverse genomic modifications in residual chromosomes

To further assess the genomic changes resulting from multiple AS chromosome cleavages induced by the M2-AS × 13 vector, six iPS cell lines were established following transfection: three retained trisomy 21 (Post-M2-AS × 13-Trisomy), and three were successfully rescued to disomy 21 (Post-M2-AS × 13-Disomy). The copy number (CN) status of these cell lines was verified using multiplex ligation-dependent probe amplification, confirming the expected CN of chromosome 21 (Fig. S4). CN estimation based on read depth within 100 K bins revealed no CN variants (Fig. 5A–C).

To evaluate off-target genomic alterations following Cas9 transfection, WGS data from the post-M2-AS × 13 cell lines was analyzed. Putative off-target loci were predicted for each gRNA sequence and compared with the detected genomic modifications. An average of 2,114 variants (range: 1,613–2,710) were detected in the Post-M2-AS × 13 cell lines, and a total of 32,413 loci (278–10,854 loci per gRNA) were predicted across the human genome (Table S2). The number of loci for which the detected variants matched predicted off-target sites was 7.3 (range: 2–14) for Post-M2-AS × 13-trisomy and 5.3 (range: 4–6) for Post-M2-AS × 13-disomy. All detected off-target endonuclease activity resulted
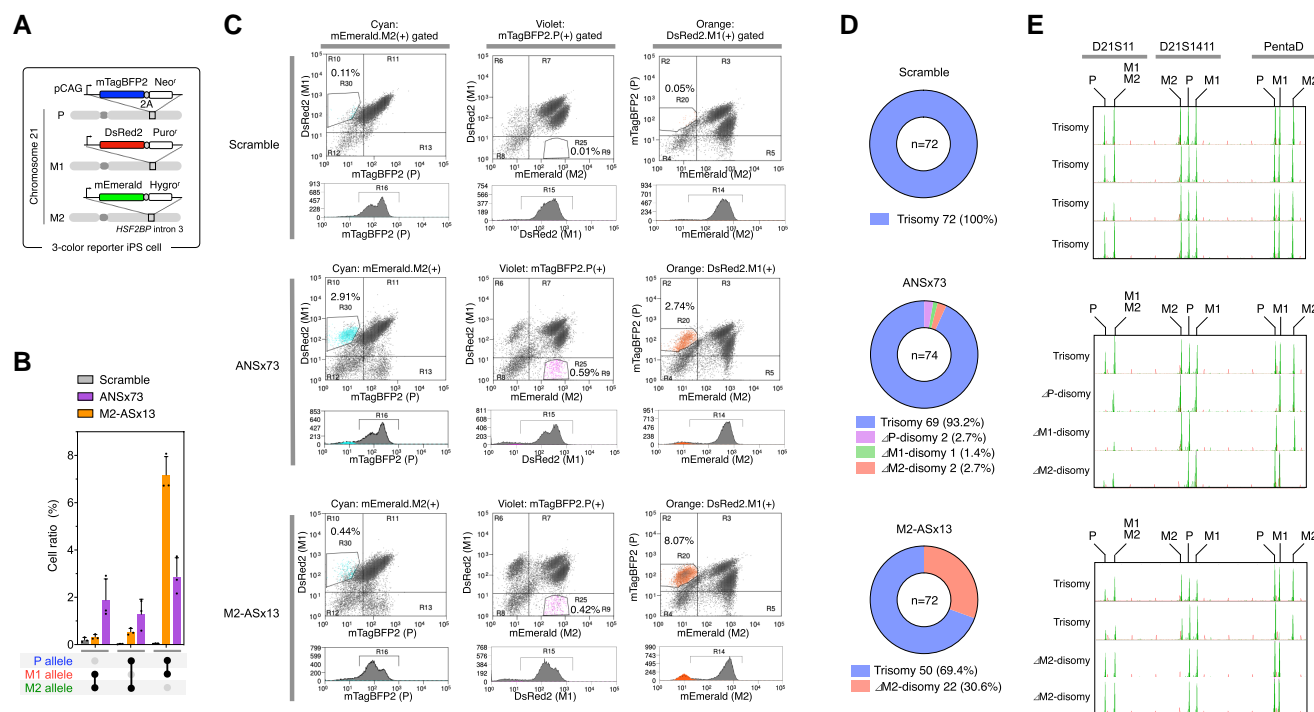
Fig. 3. Characterization of allelic loss resulting from Cas9-induced chromosomal breaks. A) Genetic scheme of the three-color reporter cell line with trisomy 21. Fluorescent protein expression cassettes for mTagBFP2, DsRed2, and mEmerald were inserted at the P, M1, and M2 alleles of chromosome 21, respectively. The loss of specific fluorescence indicates the lost allele. B) Summary of lost alleles following the Cas9-Scramble (Scramble), Cas9-ANS-DSB × 73 (ANS × 73), or Cas9-M2-AS-DSB×13 (M2-AS × 13) vector transfection into the three-color reporter cells on day 10 (n = 3 for each group). Cells that had only lost one of the three fluorescence were counted and divided by the total cells. Data are represented as mean ± SD. C) Representative views of flow cytometry assays of three-color reporter cells after transfection. D) Summary of STR analysis of lost alleles after the Scramble, ANS × 73, or AS × 13 vector transfection into the original trisomy 21 iPS cells (n = 72, 73, and 72, respectively). Single-cell cloning started 30 days after transfection in all groups. E) Representative waveforms of capillary electrophoresis for PCR amplicons of the STR loci. The repeat number at the DS21S11 locus in the M1 and M2 alleles is identical.

from gRNA pairing with nontarget alleles (P and/or M1) at on-target loci, caused by single nucleotide mismatch rather than DNA or RNA bulges. Additionally, no Cas9-induced off-target mutations were detected in genomic regions beyond the intended target loci.

To assess structural variations (SVs) induced by the M2-AS × 13 vector, the Post-M2-AS × 13 cell line bam files were analyzed using an SV caller that detects SVs larger than 15 bp. Five to six SVs were detected in Post-M2-AS × 13-trisomy strains and one SV in Post-M2-AS × 13-disomy strains (Fig. 5D and Table S3). Analysis of the 13 gRNA genomic target sites revealed 12 (92.3%) with evidence of on-target DSBs in Post-M2-AS × 13-trisomy clones. Hence, the target chromosome was cleaved at most sites but repaired and retained within the cell. Five (38.5%) of the 13 gRNA target sites showed evidence of DSBs occurring at the correct loci but on the wrong allele in Post-M2-AS × 13-disomy clones (Fig. S5).

Based on the genomic modification data at each of the 13 gRNA target sites, categorized as on-target or nontarget (Fig. S5), six gRNAs demonstrated on-target endonuclease activity without nontarget activity. Thus, a new M2-AS × 6 vector was constructed (refined-M2-AS × 6), incorporating all six gRNAs that exhibited only on-target endonuclease activity. The chromosome elimination rate, determined by FISH, using the refined-M2-AS × 6 was 13.3 ± 2.0%, which tended to be higher than that of the original M2-AS × 6 (8.4 ± 1.7%), comparable to that of the M2-AS × 8 (12.1 ± 1.2%), and lower than that of the M2-AS × 13 (17.4 ± 5.9%) (Fig. 2D). These findings suggest that the target loci quantity and

allele specificity are distinct variables influencing chromosome loss frequency.

Karyotype correction restores the gene signature

To determine if chromosomal rescue can reversibly restore gene expression profiles, RNA-seq analysis was performed on iPS cells, comparing the original trisomy 21 cells with rescued clones (Post-M2-AS × 13-disomy clone#1–3). The sample tree, generated using Pearson correlation and average linkage clustering, revealed that samples clustered according to their karyotype, forming distinct groups for trisomy and rescued disomy (Fig. 6A). Principal component analysis showed that the first principal component (67.8%) discriminated between the trisomy and rescued euploid (Fig. 6B), supporting a distinct molecular architecture. Of the analyzed 19,365 genes, 1,568 up-regulated (8.1%) and 1,305 down-regulated (6.7%) genes were identified as differentially expressed in the rescued euploid compared with the original trisomic cells (Fig. 6C and D). The gene ontology (GO) analysis of down-regulated differentially expressed genes (DEGs) in the rescued euploid showed enrichment for genes involved in metabolic processes, including ribose, cholesterol, alcohol, sterol, and some mitochondrial processes (Fig. 6E and F). Meanwhile, the up-regulated DEGs were associated with the cellular development process, nervous system development, generation of neurons, and neurogenesis (Fig. 6E). Generally, GO terms associated with down-regulated genes exhibit substantially higher false discovery rates (FDRs) compared with those of up-regulated genes, indicating that the
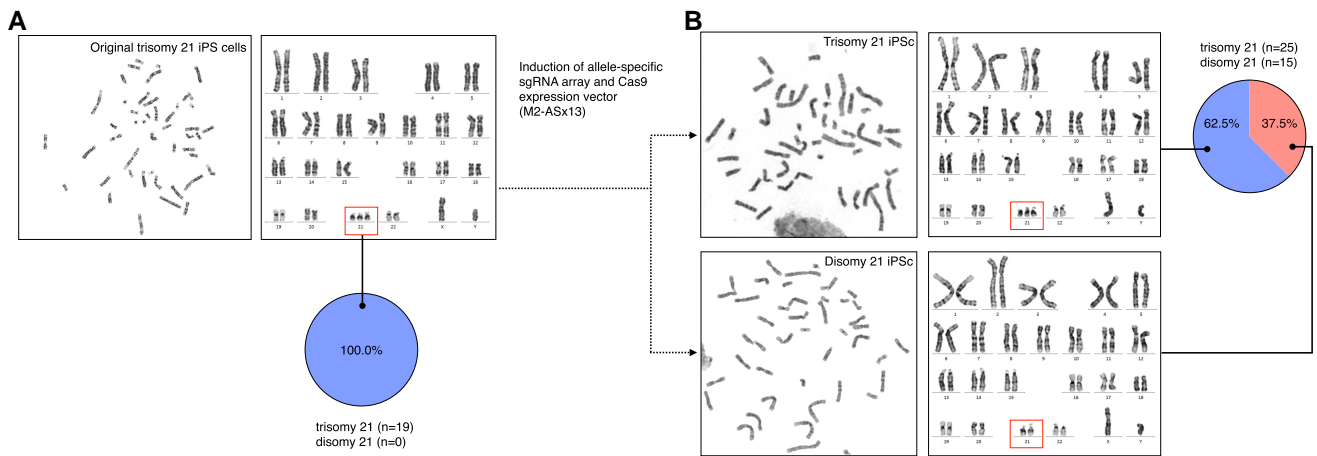
Fig. 4. Metaphase karyotype analysis using microscopy before and after treating iPS cells with the M2-AS × 13 vector. A) Metaphase capture of G-banding and karyogram of the original trisomy 21 iPS cell line. The cells show karyotypes of 47,XY,+21 in 19 (100%) out of 19 metaphases. B) Representative snapshots of metaphase after M2-AS × 13 treatment on the original trisomy 21 cells. These show karyotypes of 47,XY,+21 in 25 (62.5%) and those of 46,XY in 15 (37.5%) of 40 metaphases. G-banding analysis did not detect any apparent structural variants or additional numerical chromosomal abnormalities.
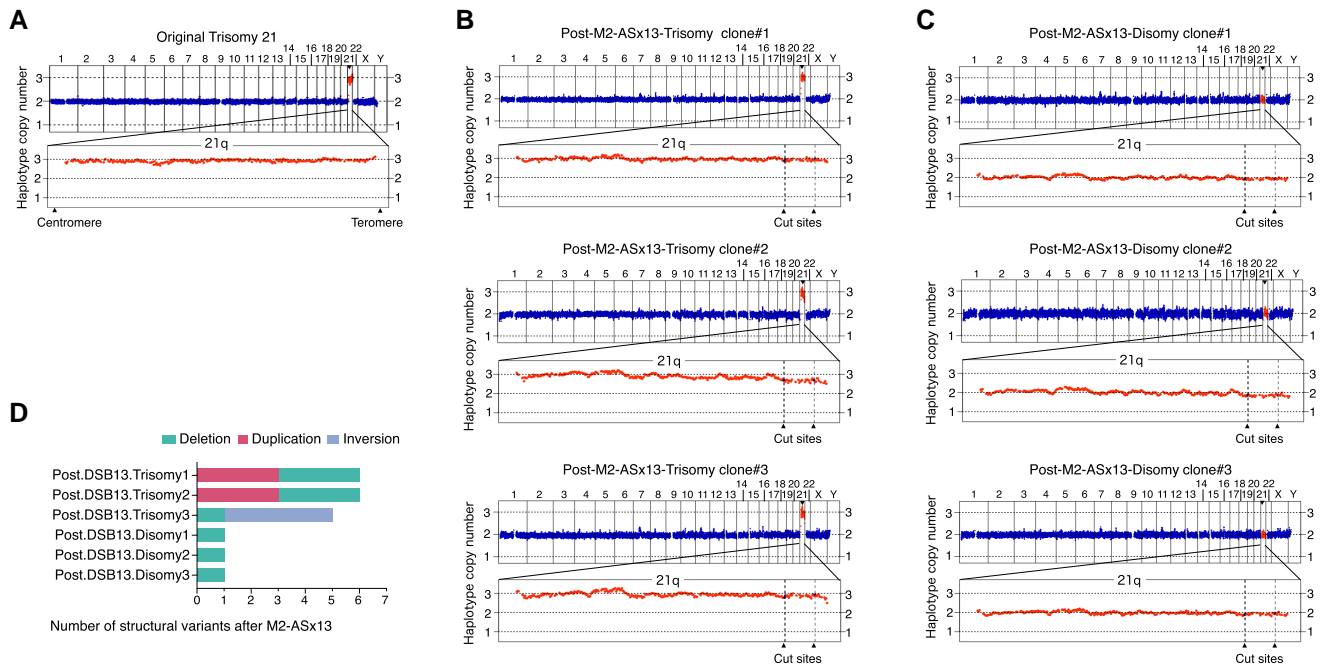
Fig. 5. Evaluation of CN and structural variants following transfection of trisomy 21 iPS cells with the M2-specific DSB×13 (M2-AS × 13) vector. A) Plot of the normalized average depth within each 100k bin for the original trisomy 21 iPS cell line. The upper panel shows all chromosomes, and the lower panel shows an expanded view of the 21q region. B) CN plots for the Post-M2-AS × 13 clones that remained trisomy 21 and C) those that were rescued to disomy 21. Arrows indicate the genomic location of the targeted cut site for the indicated gRNAs. D) Summary of structural variant analysis. All variants detected were intrachromosomal variants of chromosome 21.

GO analysis results for down-regulated genes should be interpreted with caution due to their potentially lower reliability.

DEGs were subjected to gene set enrichment analysis (GSEA) using the molecular signatures database. Rescued euploid cells were associated with enhanced gene sets that promote early development of the human central nervous system compared with trisomy 21 cells (GO:0030900 forebrain development (Fig. 6G), a part of GO:0007399 nervous system development or GO:0048731 system development, normalized enrichment score [NES] = 1.30; GO:0061351 neural precursor cell [NPC] proliferation (Fig. 6H), NES = 1.32). Considering that forebrain size defects have been detected as early as gestation week 14.7 in human DS and the reduced proliferation potency of NPCs during the embryonic period may be a leading cause of characteristic fetal brain hypotrophy in DS (16), correction of the karyotype may foreshadow subsequent modification of the organogenic features of DS at the stem-cell level. Although an enriched down-regulated region was detected on HSA21, the DEGs associated with chromosome loss were widely located across all chromosomes. This is consistent with the argument that supernumerary HAS 21 results in alterations not only in the HSA21 genes but throughout the transcriptome (Fig. S6) (17).
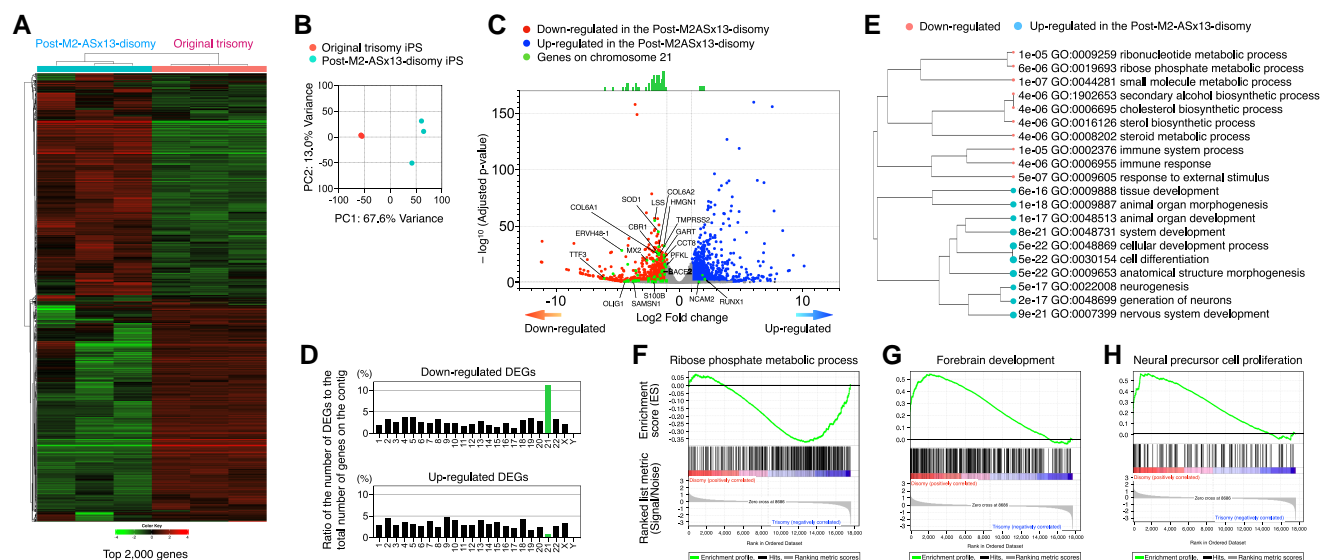
Fig. 6. Alterations in gene expression profiles between the original trisomy 21 iPS cells ($n = 3$) and M2-AS×13 vector-mediated rescued euploid cells ($n = 3$). A) Pearson correlation coefficient-based hierarchical clustering heatmap comparing gene expression patterns between the original trisomy and M2-AS×13 vector-induced euploid cells. The hierarchical clustering was performed using the 2,000 genes exhibiting the highest SD in expression levels across all samples. B) Principal component analysis of DEGs between the original trisomy 21 and M2-AS×13 vector-mediated euploid cells. C) Volcano plot depicting DEGs between the trisomy 21 and induced euploid cells. Each dot represents an individual gene. The plot shows 1,568 up- and 1,305 down-regulated genes using an adjusted P-value cutoff of 0.1 and a fold-change threshold of 2. D) Proportion of DEGs relative to the total number of genes detected on each chromosome (1 through Y). DEGs were defined as those with a log2-fold change >1.5 and an adjusted P-value < 0.01 for up-regulated genes and a log2-fold change <−1.5 and an adjusted P-value < 0.01 for down-regulated genes. E) GO enrichment analysis for biological processes, displaying the top 10 enriched gene ontologies for down-regulated and up-regulated genes, sorted by FDR. F–H) GSEA plots illustrating the enrichment of genes involved in F) ribose phosphate metabolic process, G) forebrain development, and H) NPC proliferation. NES calculated using GSEA v.4.3.2 of these gene sets are −1.16, 1.30, and 1.32, respectively. In each plot, the top portion displays the running enrichment score for the gene set along the ranked list of genes. The middle portion shows the distribution of gene set members within the ranked gene list. The bottom portion presents the values of the ranking metric across the ranked gene list.

The gene signature data set was compared between isogenic iPS cells derived from monozygotic twins discordant for trisomy 21 to assess the similarity between the transcriptomic alteration in this study and those commonly seen in the literature (17, 18). Strikingly, GO enrichment analysis with up-regulated DEGs calculated using the same pipelines showed that nine of the top 10 GO terms (90%) matched when ranked by FDR (Fig. S7). This supports the hypothesis that extra-chromosome removal rescues trisomy 21 phenotypes regarding integrated gene signature alteration. Tissue expression analysis using TISSUE 2.0 and common tissue-expression profile data sets revealed that the top 10 tissues were related to the central nervous system or ectoderm (Table S4). This suggests that genes up-regulated by chromosome loss were significantly associated with genes expressed in the nervous system or the nervous system during development, even in the pluripotent stem-cell stage.

AS chromosome cuts also trigger chromosome loss in terminally differentiated cells

Although the human body contains various somatic stem cells, from which all differentiated cells originate, most are mature, terminally differentiated cells. Thus, investigating whether chromosome elimination can also occur in differentiated cells is crucial for understanding the potential scope of this technique. Accordingly, the effects of AS multiple DSBs were evaluated on terminally differentiated cells with trisomy 21. To assess the chromosome elimination rate in differentiated cells, the M2-AS×13 vector was transfected into skin-derived primary fibroblasts, the source of the iPS cells used in this study (Fig. 7A). The chromosome elimination rate was 0.42 ± 0.68, 1.4 ± 0.83,

and 13.9 ± 4.2 for untreated, Scramble, and M2-AS×13 vectors, respectively (Fig. 7B–D). These findings demonstrate that AS multiple chromosome cuts can potentially induce effective chromosome elimination in differentiated cells.

Subsequently, to explore whether chromosome elimination can occur in nondividing cells, an experimental system was employed in which 5-ethynyl-2′-deoxyuridine (EdU)—a thymidine analog—was continuously added to the fibroblast medium. Notably, a 3.2% chromosome elimination rate was observed in nondividing cells that had not incorporated EdU, considerably higher than the 0.4% rate observed in the Scramble control (Fig. S8). While not directly comparable to the 13.9% rate in experiments using media supplemented with 10% fetal bovine serum (FBS; Fig. 7D), this supports the hypothesis that chromosome elimination can be induced even in nondividing cells using the proposed method. Importantly, throughout the CRISPR/Cas9 transfection experiments conducted using iPS cells and fibroblasts, no chromosome 21 gains were detected.

Karyotype correction improves the iPS cell phenotype

To understand whether karyotype correction can reversibly improve the cellular phenotype, the cell proliferation rates of the original trisomy 21 and rescued clones (Post-M2-AS×13-disomy clones #1–3) were evaluated. The rescued clones exhibited a slight increase in proliferation rate compared with the trisomy clones (Fig. S9A), and the doubling time was remarkably shorter in the rescued clones (Fig. S9B). Additionally, mitochondrial dysfunction in trisomy 21 iPS cells reportedly leads to excessive production of reactive oxygen species (ROS), which is thought to be involved in
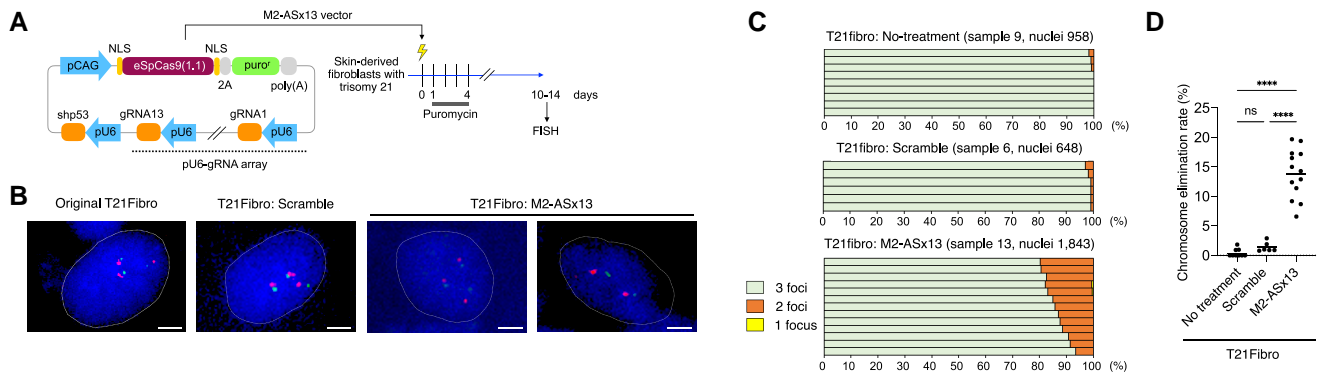
Fig. 7. CRISPR/Cas9-mediated trisomy rescue in fibroblasts derived from individuals with trisomy 21. A) Experimental design for introducing expression vectors into trisomy 21 fibroblasts. B) Representative FISH images of interphase nuclei. Scale bars: 5 μm. C) Chromosomal composition of cells in the untreated control (No treatment, $n = 9$), Scramble control ($n = 6$), and M2-AS×13 treatment ($n = 13$) groups. Each bar represents an independent experiment, indicating the percentage of cells displaying each chromosomal complement ($n = 102$–206 cells per cell line). The total number of cells analyzed was 958 for the No treatment, 648 for the Scramble, and 1,843 for the M2-AS×13 treatment group. D) Chromosome elimination rate (%) determined by quantifying FISH signals. Asterisks indicate statistical significance. ****$P < 0.0001$.

regulating programmed cell death (19). Therefore, ROS production was quantitatively evaluated in the original trisomy 21 and rescued clones. ROS production was markedly reduced in the rescued clones (Fig. S10). Collectively, these observations indicate that chromosome elimination can reversibly improve cellular fitness.

Discussion

Identifying the specific set of genes on HSA21 responsible for the clinical DS phenotypes has proven more challenging than initially anticipated. Currently, consensus regarding the gene expression changes specific to trisomy 21 based on gene signature analyses is lacking. This inconsistency is primarily attributed to the strong influence of individual genetic variability on expression profiles (17, 20, 21). Interindividual genetic differences can significantly impact the transcriptional landscape, impeding the identification of consistent and reliable gene expression patterns unique to this condition. Herein, the DEGs identified in this study were compared with those of a previously reported dataset derived from isogenic iPS cells of monozygotic twins discordant for trisomy 21 (17, 18). Using the same analytical pipelines, only partial agreement was observed between the two datasets, with 518/1,568 (33.0%) up-regulated and 393/1,305 (30.1%) down-regulated DEGs overlapping. This low concordance rate suggests that differences in individual genetic backgrounds may be critical in shaping the gene expression profiles associated with trisomy 21. This complexity of the genetic alterations in DS presents a formidable challenge for developing targeted therapies.

The aneuploidy-associated phenotype hypothesis has been recently proposed, suggesting that gaining an extra copy of a chromosome causes gene-driven and aneuploidy-driven phenotypes independent of the genes encoded within that chromosome (22). The conserved aneuploidy-associated phenotypes, such as reduced viability, aberrant nuclear morphology, and elevated metabolic demand, are observed across various organisms, from yeast to human cells (20). Therefore, inducing trisomy rescue to restore the normal diploid state through the loss of genetic material may be a radical yet effective strategy to resolve the phenotypic issues arising from trisomy.

However, inducing total chromosome loss or silencing has proven remarkably challenging from a technical standpoint. Attempts have been made to eliminate excess chromosomes by inserting the lethal transgene TK-NEO (23) or to silence the extra chromosome by inserting the X-chromosome inactivation gene (XIST) into a single HSA21 (24). However, both methods require genome modification and are thus incompatible with clinical use. In contrast, our strategy of specifically cleaving the target chromosome allele and eliminating the entire target chromosome from the cell is advantageous as it is simpler than these other methods.

Genome editing using CRISPR/Cas9 reportedly causes massive chromosome deletions and, rarely, loss of entire chromosomes (8, 25). Whole chromosome loss is generally discussed in the context of the serious and potentially fatal side effects of CRISPR/Cas9-based gene therapy attempts (26). Our strategy harnesses this side effect as the fundamental principle for targeted chromosome elimination. However, even in the case of AS targeting, Cas9-mediated whole chromosome loss in euploid cells has been largely limited to human or mouse preimplantation zygotes. Meanwhile, it is uncommon in other experimental settings, such as cultured stem cells (27). Diploid animal cells with normal karyotypes result in monosomic cells when autosomal chromosome loss occurs, which can be detrimental to survival. Consequently, obtaining cells that have undergone whole chromosome loss in the case of normal karyotypes is challenging. While karyotypic stability is typically maintained in trisomic cells, reprogramming to iPS cells can induce trisomy-biased chromosome loss (TCL) (28, 29). Our method capitalizes on this by employing chromosome-specific DSB stimuli to target and eliminate excess chromosomes. Evidence that Cas9-induced chromosome cleavage in euploid cells results in truncation (terminal deletion) on the telomere side from the cleavage point has been reported for autosomal ANS (25), autosomal AS (27), and chromosome Y AS cuts (8). In contrast, we did not detect terminal deletions in trisomic cells; instead, whole chromosomes were eliminated. This discrepancy may be attributed to TCL or may simply result from enrichment due to differences in cellular fitness.

The present study, however, demonstrated that Cas9-induced DSBs resulted in genomic alterations, such as indels and relatively small SVs, which are undetectable by G-banding chromosome analysis. Although all lost chromosomes were the intended target chromosomes of the CRISPR/Cas9 system, as long as the chromosome elimination rate is not 100%, mutations will be introduced into the cells on the residual target chromosomes (i.e. the target chromosomes that were cleaved but repaired and retained within

the cells). Thus, increasing the chromosome elimination rate will be effective in reducing the overall burden of genetic modifications.

The temporary artificial suppression of DNA repair mechanisms following DNA cleavage, specifically the siRNA-mediated knockdown of LIG4 and POLQ, contributed to the improvement of postcleavage chromosome elimination rates in the present study. Hence, suppressing DNA damage repair promotes target chromosome elimination from cells rather than its retention, possibly by increasing unrepaired double-strand breaks. Furthermore, these results suggest that a minimum of 48 h, which corresponds to the duration of POLQ and LIG4 knockdown, is necessary for cells to determine whether to eliminate or retain the cleaved chromosomes. This finding highlights the critical role of DNA repair pathways in the fate of damaged chromosomes and provides valuable insights into the time frame required for cellular decision-making processes regarding chromosome stability.

Previously reported methods to directly eliminate specific human chromosomes or delete most of a chromosome can be divided into two main categories: nuclease-mediated and nuclease-dead Cas9 (dCas9) approaches to tether a certain protein to a chromosome of interest (30). Nuclease-mediated approaches include the Cas9 system with one or multiple chromosome-specific sgRNAs wherein one or multiple DNA DSBs are induced in the arm (8, 9, 25, 31) or the (peri-)centromeric region of the targeted chromosome (32, 33), leading to whole or partial loss of the targeted chromosome. Other such approaches include a combination of centromere-proximal and centromere-distal DSBs (34) or artificial telomere sequence incorporation into the peri-centromere (33, 35). However, one additional step of genome editing is required for arm loss. In contrast, other methods utilize the fusion of dCas9 with the motor and stalk domain of microtubule minus-end-directed motor protein Kinesin 14VIb (36), CENP-T$^{1-243}$, inducing ectopic kinetochore assembly (37), or mutant kinetochore proteins, which may induce a pseudo-merotelic kinetochore attachment (38). These proteins cause the targeted chromosome to lag and consequently missegregate during anaphase, resulting in its respective gain and loss in daughter cells. Although the dCas9-based approaches are attractive for avoiding DSBs, which may result in unanticipated critical genomic alterations (15), they cannot control whether to gain or lose the target chromosomes. Furthermore, among these approaches, KaryoCreate—a recently reported sophisticated chromosome elimination technique utilizing the dCas9 system—is unable to target chromosome 21 due to the absence of specific repetitive sequences in the pericentromeric region suitable for gRNA design (38). Most importantly, while these Cas9- or dCas9-based advanced methods target specific chromosomes, they ignore ploidy. In normal human somatic cells, each chromosome-specific gRNA targets two sites, one on each autosomal homolog. However, in trisomy or cancer cells, the same gRNA targets three or more sites due to additional chromosome copies. Hence, the AS method boasts major advantages, as it targets a single unique chromosome, enabling efficient elimination. The importance of allele specificity in targeting also cannot be understated to avoid the generation of uniparental disomy.

Genes expressed in terminally differentiated or differentiating cells are generally thought to be silenced in iPS cells. However, gene expression analysis using isogenic euploid and trisomic iPS cell pairs for chromosome 21 revealed differences during organ development and cell differentiation (17). Furthermore, genes associated with trisomy 21-induced phenotypes at the cellular and organismal levels, particularly those involved in nervous system development, exhibit positive enrichment of euploidy in iPS cells

(17, 39, 40) and embryoid bodies (41). Although directly proving the relationship between gene expression in iPS cells and the phenotype of differentiated cells or individuals is challenging, our GO analysis suggests that karyotype normalization of trisomy 21 cells may reversibly restore the corrected gene signature. The downregulation of genes involved in the metabolic process observed in the induced euploid cells in the present study may correlate with the previous finding that an extra chromosome 21 homolog causes systemic hypermetabolism in a transchromosomic mouse model (TcMAC21) harboring a near-complete human chromosome 21 (42). On the contrary, the upregulation of nervous-system-related genes observed in the induced euploid cells in the present study may suggest a restoration of the transcriptional signature responsible for the DS phenotype, given that neuroanatomical abnormalities and cognitive impairment are evident in most DS individuals (43).

Trisomy 21 embryos arise from meiotic nondisjunction during gametogenesis. In the case of the first meiotic nondisjunction, all three copies of chromosome 21 are genetically distinct. Most trisomy 21 in DS is caused by nondisjunction during the first meiotic division of oogenesis (44). Consequently, even when recombination occurs between homologous chromosomes, each of the three copies of HSA21 typically possesses unique gRNA targets. This characteristic offers the advantage of targeting only one of the three HSA21 copies.

Although the current research concept may become an important area of future investigation, it includes challenges that must be addressed for in vivo application. First, when the target chromosome is not eliminated by Cas9 treatment, variants are introduced into the remaining target chromosome, and crucially, the target genome is replaced by a sequence no longer recognizable by the employed gRNA. Second, unexpected endonuclease activity is observed at the nontarget allele even when the target chromosome is lost. Thus, protecting nontarget alleles from Cas9-induced DSBs is a major challenge. These issues may be addressed by epigenomic approaches that do not induce DSBs. Third, this study focused on subtelomere targeting and lacks insight into how targeting other chromosomal regions and their combinations, such as centromeres and peri-centromeres, affects chromosome elimination efficiency. Fourth, the phasing method we employed could potentially be simplified by replacing short-read sequencing with long-read techniques. Fifth, the current study is limited by the use of only a single iPS cell line and two cell types (iPS cells and fibroblasts) in the experiments. While our findings provide proof-of-concept for the method, evaluating the approach in clinically relevant cell types, such as neurons and glial cells, would greatly enhance its potential for translational applications. However, these additional experiments are beyond the scope of the current study and represent important avenues for future research. Sixth, WGS analysis was not performed on cells after all treatments, including Scramble control, M2-AS × 1 to M2-AS × 12, ANS series, or refined-M2-AS × 6. Consequently, comprehensive information on genome modifications across all cells used in the experiments may not be sufficient. Seventh, the present study does not investigate the impact of genes involved in the DSB repair mechanism, other than LIG4 and POLQ, on the rate of chromosome elimination. Eighth, our study did not include a quantitative assessment of protein depletion following siRNA treatment, which would have provided additional confirmation of the knockdown efficiency beyond the mRNA-level evaluation using digital PCR. Finally, this study emphasizes the results of karyotype correction by chromosome cutting without adequately addressing the factors

determining chromosome repair versus loss. Future research directions include understanding how Cas9-treated chromosomes are lost and the consequences of Cas9-treated chromosomes remaining in the genome.

In conclusion, this study showcases the potential of employing an AS CRISPR/Cas9 approach to effectively correct the chromosomal abnormality in human trisomy 21 cells by selectively removing the extra copy of chromosome 21, demonstrating the feasibility and efficacy of this strategy as a therapeutic intervention for DS. By employing a comprehensive AS Cas9 target sequence extraction method, we successfully developed a strategy that efficiently removes the target chromosome, highlighting the practicality of this approach for therapeutic interventions. Furthermore, we demonstrated that transient suppression of DNA damage response genes enhances the chromosome loss rate, and the chromosomal rescue reversibly restores both gene expression and cellular phenotypes. Notably, this approach is effective not only in pluripotent stem cells but also in differentiated cells, and chromosome elimination was achieved in both dividing and nondividing cells, underscoring its broad therapeutic potential. While further optimization, coupled with additional experiments to establish reproducibility and safety, including assessments of broader applicability through more comprehensive WGS analysis, is necessary, our findings provide a foundation for the development of innovative therapeutic interventions targeting trisomy 21. Future research should focus on further improving the chromosome elimination rate and developing methods that do not rely on DSBs. The development of in vivo delivery systems also warrants further exploration. Ultimately, the insights gained from this study contribute to the ongoing efforts to address the fundamental genetic cause of DS and pave the way for more sophisticated medical interventions in the future.

Materials and methods
Ethical statement
The study protocol was approved by the Institutional Review Board of Mie University Graduate School of Medicine, Japan (approval number: 1578). Skin-derived fibroblasts were obtained from a 1-y-old boy diagnosed with complete trisomy 21 during a medically necessary surgical procedure at Mie University Hospital, Tsu, Japan, in March 2016. Written informed consent was obtained from the patient's parents before the procedure. The study adhered to the guidelines outlined by the Declaration of Helsinki. To determine the parental origin of HSA21 in the trisomic cell line, buccal swabs (GE Healthcare, Piscataway, NJ, USA) were also collected from the patient's parents for STR analysis.

Cell culture
The iPS cells were maintained feeder-free (45) and uncoated (46) using StemFit AK03 medium (Ajinomoto, Tokyo, Japan) containing 0.25 µg/cm^2 iMatrix-511 (#892012, Nippi, Tokyo, Japan). The medium was supplemented with 10 µM Y-27632 (#253-00513, Nakalai Tesque, Kyoto, Japan) for 24 h only during cell passaging. For passaging, the cells were dissociated into single cells by treatment with 0.5× TrypLE Select (1× TrypLE Select [#A1285901, Thermo Fisher Scientific] diluted 1:1 with 0.5 mM EDTA [#06894-14, Nakalai Tesque, Kyoto, Japan] in phosphate-buffered saline) for 4 min at 37 °C (45). The cells were scraped under StemFit and dissociated into single cells by pipetting and plated into the noncoated wells of a 6-well cell culture plate (#353046, Corning) or 10-cm cell culture dish (#353003, Corning) in media

volumes of 1.5 and 9.0 mL, respectively. The medium was renewed every other day. Skin primary fibroblasts were maintained in Dulbecco's modified eagle medium (#12800017, Gibco) supplemented with 10% FBS (#10270106, Gibco), 3.7 g/L sodium bicarbonate, 100 units/mL penicillin, 100 µg/mL streptomycin, and 250 ng/mL amphotericin B (#15240062, Gibco), with medium changes approximately every 2 days. All fibroblasts used in the experiments did not exceed passage nine from the initial culture.

AS Cas9 target selection from WGS results
From processed clean reads of the WGS data set, all 20 contiguous sequences with downstream NGG (N can be A, G, C, or T) or upstream CCN were extracted using an in-house script (zsh 5.7.1). Theoretically, Cas9 recognition sequences specific to a single allele disappear only in the cell line where the allele has been deleted. Thus, AS Cas9 recognition sequences were extracted by the following set operation: a set of candidates for the P-allele-specific sequences, T21 ∩ ΔM1 ∩ ΔM2 \ ΔP; M1-allele specific, T21 ∩ ΔP ∩ ΔM2 \ ΔM1; and M2-allele specific, T21 ∩ ΔP ∩ ΔM1 \ ΔM2; where T21, ΔP, ΔM1, and ΔM2 are sets of Cas9 recognition sequences extracted from all cleaned reads of each cell line, respectively. This method also avoids mapping failures caused by fast mapping algorithms (e.g. bwa). Using these candidate sequences, 150-length sequences were recursively obtained from the original cleaned-up fastq format file and mapped to a hg38 human reference sequence using blastn (v2.14.0+). The sequences mapped to the HSA21 primary assembly (i.e. not alt-loci) were retained. Sequences containing more than a four-thymidine stretch (poly-T U6 promoter termination signal) or six or more repeats of the same base (e.g. AAAAAA) were excluded. In the 20 bases recognized by Cas9, excluding the PAM sequence, if any single base mismatch was matched to other loci across all chromosomes, the corresponding gRNA candidates were excluded. Subsequently, for each candidate sequence, filtering was performed under the condition that the number of reads, including the sequence, was ≥5 for cell lines that theoretically contained the target allele and ≤1 for cell lines that theoretically did not contain the target allele. The genomic region 5 Mb before the telomere (chr21: 41,699,982–46,699,982 on build GRCh38) was defined as a subtelomere (47).

ANS Cas9 targets
For ANS but HSA21-specific tandem repeat loci, gRNA sequences of 5′-CTGTGAGCATCCTCTGTGGA(NGG)-3′ (24 repeats spanning 46,169,326 through 46,170,865, referred to as ANS × 24 in this study), 5′-GGAGGCTCGGTGCAGGTAAG(NGG)-3′ (49 repeats spanning 42,587,468 through 42,590,295 on build GRCh38.p14, ANS × 49), and a combination of (ANS × 73) were used (9). As these targets are ANS, the number of targets per trisomy 21 cell was 72 for ANS × 24, 147 for ANS × 49, and 219 for ANS × 73. Both target sequences are located in the q-arm subtelomeric region of HSA21. The presence of these sequences in the cell lines was confirmed by counting the reads containing them using WGS results.

Construction of multicistronic expression plasmid vectors for Cas9 and gRNAs
The puromycin-resistant gene was PCR amplified from the pLenti PGK v5-LUC Puro plasmid (Addgene plasmid #19360). The T2A-puro sequence was then cloned into the FseI restriction site on eSpCas9(1.1) (Addgene plasmid #71814), a px330-like plasmid expressing high specificity SpCas9 with K848A, K1003A, and R1060A mutations (48). The human U6 polymerase III promoter-driven shp53 module was PCR amplified from pCXLE-hOCT3/

4-shp53-F (Addgene plasmid #27077) and cloned into the XbaI site of eSpCas9(1.1). The CAG promoter (consisting of a CMV early enhancer element, the chicken β-actin gene promoter, and the rabbit β-globin gene splice acceptor) was PCR amplified from pCAG-Cre (Addgene plasmid #13775). The CBh promoter sequence between KpnI and AgeI was replaced with the CAG promoter sequence (CAG-eSpCas9(1.1)-2A-puroR_U6-shp53_empty). Plasmids expressing gRNA for AS target sequences were prepared by ligating oligonucleotides (custom synthesized by Fasmac, Kanagawa, Japan) into the BbsI site of eSpCas9(1.1). The U6-gRNA expressing module was PCR amplified and cloned into pCAG-eSpCas9(1.1)-2A-puroR_U6-shp53_empty for the first pU6-gRNA module insertion. The second and subsequent U6-gRNA modules were constructed individually, PCR amplified, and inserted into the cloning intermediates to obtain the gRNA-Cas9 coexpressing vectors. All PCR amplicons were electrophoresed, extracted from an agarose gel, and purified using a Qiaquick gel extraction kit (Qiagen). All cloning processes were performed using the Gibson assembly method (#E2621, NEBuilder HiFi DNA Assembly Master Mix, New England Biolabs), excluding oligo ligation (#M2200S, Quick ligation kit, New England Biolabs). All insertion sites of PCR-amplified fragments were confirmed by direct sequencing using the Sanger method. The 5′-CCGGGTCTTCGAGAAGACCTNGG-3′ sequence was used as a Scramble gRNA target sequence that does not exist in the human genome (GRCh38.p14). The off-target finder software Cas-OFFinder confirmed that the Scramble gRNA sequence had no human genomic target sites within 2 bp mismatches (49). Before transfection into iPS cells, plasmids were amplified in Stellar competent cells (#636763, Takara-Clontech, Shiga, Japan), NEB Stable cells (#C3040, New England Biolabs Japan, Tokyo, Japan), and VB UltraStable cells (#UC001, VectorBuilder Japan, Kanagawa, Japan) and purified as endotoxin-free plasmid DNA (#740412.10, NucleoBond Xtra Midi Plus, Macherey-Nagel, Dueren, Germany).

Transfection of a Cas9-gRNAs co-expression vector into trisomy 21 cells

Cultured iPS cells with trisomy 21 were dissociated into single cells using 0.5× TrypLE Select in the presence of a 10 μM Y-27632. Subsequently, 0.5–1.0×10^6 cells were suspended in 100 μL of Resuspension Buffer R supplemented with 16 μg of Cas9–gRNA coexpression vector and 0.6 μM B18R protein (#VRP-0366, LD Biopharma) with or without siRNAs. Silencer Select siRNAs (Life Technologies, Japan) against LIG4 (#s8179) and POLQ (#s21059) were used at a final concentration of 0.25 μM. The cells were electroporated using 100 μL of the Neon Transfection System at 1,200 V, 20 ms, and 2 pulses. The electroporated cells were plated in a 6-well plate with StemFit AK03 medium containing iMatrix-511 at 0.25 μg/cm² and 10 μM Y-27632. To enrich plasmid-transfected cells, short-term drug selection with puromycin (1.0 μg/mL, #A1113802, Gibco) was initiated on the day following electroporation for 3 days. On day 4 post-transfection, the medium was replaced with a fresh StemFit without puromycin. On days 5–10, the resulting cells were dissociated for FISH analysis or G-banding examination to measure the target chromosome elimination rate or were further expanded for single-cell cloning for STR analysis. iPS cells were grown 10–17 passages before the FISH step and 15 passages before the G-banding or STR analysis. For transfection into skin-derived primary fibroblasts, cells were dissociated using trypsin-EDTA (#204-16935, Fujifilm Wako chemicals). Then, 0.5×10^6 cells were suspended in 100 μL of Resuspension Buffer R with 16 μg of the vector, B18R protein, and siRNAs (LIG4 and POLQ) at the same concentration used for iPS cells. Electroporation parameters of 1,650 V, 10 ms, and three pulses were used. The fibroblast culture media used 1 day before and after electroporation was free of antibiotics and antimycotic agents. The fibroblasts were fixed 17–20 days after electroporation for FISH analysis.

DNA FISH

The iPS cells cultured in a 6-well plate were harvested with TrypLE select (Thermo Fisher Scientific, Waltham, MA, USA). Cells were then treated with Buffered Hypotonic Solution (#GGS-JL006, Genial Helix, Flintshire, UK) at 37 °C f or 15 min, fixed with a 3:1 (v/v) ethanol-acetic acid solution, and added dropwise to glass slides (Matsunami, Osaka, Japan). The slides were left to air-dry overnight, dehydrated through an ethanol series (70% at −20 °C, 90, and 100% at room temperature for 5 min each), and air-dried. Three HSA21-specific DNA probes, produced from the BAC clone #RP11-15E10, #RP11-777J19, and #RP11-640F21 (BACPAC Resources Center, Emeryville, CA, USA) using DIG-Nick Translation Mix and Biotin-Nick Translation Mix (Roche, Darmstadt, Germany), hybridized to 21q21.1, 21q22.13, and 21q22.3, respectively, were used. The probes were denatured in a heat block at 80 °C for 10 min, followed by immediate cooling on ice for 5 min. The slides were hybridized in a humidified chamber at 37 °C for approximately 16 h and washed with 50% (v/v) formamide in 2× saline sodium citrate (SSC) at 45 °C for 5 min thrice, 0.8× SSC at 61 °C for 5 min thrice, followed by blocking in 4× SSC with 3% bovine serum albumin (BSA) and 0.2% Tween-20 at 37 °C for 30 min. The digoxigenin-labeled DNA probe (#RP11-777J19 or #RP11-640F21) was detected with an antidigoxigenin-rhodamine complex (1/100, Roche). The biotin-labelled DNA (#RP11-15E10) was detected using streptavidin-conjugated Alexa Fluor 488 (1/200, Thermo Fisher Scientific, Waltham, MA, USA) in 4× SSC with 3% BSA and 0.2% Tween-20 for 30 min at 37 °C. Metaphase and interphase images were digitally captured using a BZ-X700 all-in-one fluorescence microscope (Keyence, Osaka, Japan) and processed using the BZ-H3A software provided with the microscope. When the same number of spots was observed for two colors, the spots per color were enumerated, representing the number of chromosome 21 copies per cell.

Statistical analysis

All statistical evaluations were performed using GraphPad Prism 9 software (v9.4.0, GraphPad Software, San Diego, CA, USA), and quantitative values are expressed as mean ± SD. The Kolmogorov–Smirnov test for normality was performed for each data set to determine the appropriate statistical testing procedure. Analysis was performed using a one-way ANOVA with Bonferroni correction. All correlations were performed using the Pearson correlation coefficient. Statistical significance was defined at $P < 0.05$. Graphs were generated using GraphPad, Prism 9, or R packages.

External data used in this study

To compare transcriptome differences between isogenic trisomy 21 and euploid iPS cells, experimental RNA-seq raw data (fastq) of isogenic human iPS cells derived from twin individuals discordant for trisomy 21 reported by Hibaoui et al. (17) were downloaded from the Sequence Read Archive (Accession: PRJNA227902) (17, 18). These data were reanalyzed using the same pipelines presented above.

Supplementary Material

Supplementary material is available at *PNAS Nexus* online.

Author Contributions

R.H.: conceptualization, data curation, formal analysis, funding acquisition, methodology, investigation, project administration, resources, software, visualization, writing—original draft, writing—review & editing. S.W.: funding acquisition, methodology, investigation, writing—review & editing. H.S.: supervision. S.T.: methodology, supervision, writing—review & editing. Y.K.: methodology. Y.M.: data curation, methodology, writing—review & editing. Y.S.H.: supervision. H.I.: data curation, investigation, supervision. H.K.: supervision.

Data Availability

We deposited the trisomy 21 iPS cell line [47,XY,+21] (HPS4270) and three disomy 21 iPS cell lines [46,XY] (HPS4271, HPS4272, and HPS4273) in the RIKEN BioResource Research Center (Ibaraki, Japan). The WGS and RNA-seq data generated in this study have been deposited in the Sequence Read Archive under BioProject with the accession code PRJNA899979. The source data for Figs. 1C, 2D, E, 2G–I, 3B, 5A–C, 6A–H, 7C, D, S2, S3C, S8F, S9A, B, and S10B are available in Data set S1. Previously published data (Sequence Read Archive, accession; PRJNA227902) were used for this work. The computational pipeline for extracting allele-specific SpCas9-system recognition sequences is publicly available on GitHub (https://github.com/RayHashizume/Allele-specific-Cas9TargetExtract.git).

References

1   Stallings EB, *et al.* 2024. National population-based estimates for major birth defects, 2016–2020. *Birth Defects Res.* 116(1):e2301.

2   Antonarakis SE, *et al.* 2020. Down syndrome. *Nat Rev Dis Primers.* 6(1):9.

3   Abukhaled Y, Hatab K, Awadhalla M, Hamdan H. 2024. Understanding the genetic mechanisms and cognitive impairments in Down syndrome: towards a holistic approach. *J Neurol.* 271(1):87–104.

4   Zampieri BL, Costa ACS. 2022. Evidence of energy metabolism alterations in cultured neonatal astrocytes derived from the Ts65Dn mouse model of Down syndrome. *Brain Sci.* 12(1):83.

5   Kazuki Y, *et al.* 2022. A transchromosomic rat model with human chromosome 21 shows robust Down syndrome features. *Am J Hum Genet.* 109(2):328–344.

6   Dahdouh EM. 2021. Preimplantation genetic testing for aneuploidy: a review of the evidence. *Obstet Gynecol.* 137(3):528–534.

7   Miyata M, Yoshida J, Takagishi I, Horie K. 2023. Comparison of CRISPR-Cas9-mediated megabase-scale genome deletion methods in mouse embryonic stem cells. *DNA Res.* 30(1):dsac045.

8   Adikusuma F, Williams N, Grutzner F, Hughes J, Thomas P. 2017. Targeted deletion of an entire chromosome using CRISPR/Cas9. *Mol Ther.* 25(8):1736–1738.

9   Zuo E, *et al.* 2017. CRISPR/Cas9-mediated targeted chromosome elimination. *Genome Biol.* 18(1):224.

10 Allach El Khattabi L, *et al.* 2019. A genome-wide search for new imprinted genes in the human placenta identifies DSCAM as the first imprinted gene on chromosome 21. *Eur J Hum Genet.* 27(1):49–60.

11 Omori S, *et al.* 2017. A pair of maternal chromosomes derived from meiotic nondisjunction in trisomy 21 affects nuclear architecture and transcriptional regulation. *Sci Rep.* 7(1):764.

12 Wakita S, *et al.* 2022. Experimental method for haplotype phasing across the entire length of chromosome 21 in trisomy 21 cells using a chromosome elimination technique. *J Hum Genet.* 67(10): 565–572.

13 Schep R, *et al.* 2021. Impact of chromatin context on Cas9-induced DNA double-strand break repair pathway balance. *Mol Cell.* 81(10):2216–2230.e10.

14 Saito S, Maeda R, Adachi N. 2017. Dual loss of human POLQ and LIG4 abolishes random integration. *Nat Commun.* 8:16112.

15 Leibowitz ML, *et al.* 2021. Chromothripsis as an on-target consequence of CRISPR-Cas9 genome editing. *Nat Genet.* 53(6):895–905.

16 Stagni F, Bartesaghi R. 2022. The challenging pathway of treatment for neurogenesis impairment in Down syndrome: achievements and perspectives. *Front Cell Neurosci.* 16:903729.

17 Hibaoui Y, *et al.* 2014. Modelling and rescuing neurodevelopmental defect of Down syndrome using induced pluripotent stem cells from monozygotic twins discordant for trisomy 21. *EMBO Mol Med.* 6(2):259–277.

18 Letourneau A, *et al.* 2014. Domains of genome-wide gene expression dysregulation in Down's syndrome. *Nature.* 508(7496): 345–350.

19 Liu Y, Zhang Y, Ren Z, Zeng F, Yan J. 2023. RUNX1 upregulation causes mitochondrial dysfunction via regulating the PI3K-Akt pathway in iPSC from patients with Down syndrome. *Mol Cells.* 46(4):219–230.

20 Hwang S, *et al.* 2021. Consequences of aneuploidy in human fibroblasts with trisomy 21. *Proc Natl Acad Sci U S A.* 118(6): e2014723118.

21 Zhu PJ, *et al.* 2019. Activation of the ISR mediates the behavioral and neurophysiological abnormalities in Down syndrome. *Science.* 366(6467):843–849.

22 Torres EM. 2023. Consequences of gaining an extra chromosome. *Chromosome Res.* 31(3):24.

23 Li LB, *et al.* 2012. Trisomy correction in Down syndrome induced pluripotent stem cells. *Cell Stem Cell.* 11(5):615–619.

24 Jiang J, *et al.* 2013. Translating dosage compensation to trisomy 21. *Nature.* 500(7462):296–300.

25 Papathanasiou S, *et al.* 2021. Whole chromosome loss and genomic instability in mouse embryos after CRISPR-Cas9 genome editing. *Nat Commun.* 12(1):5855.

26 Turocy J, Adashi EY, Egli D. 2021. Heritable human genome editing: research progress, ethical considerations, and hurdles to clinical practice. *Cell.* 184(6):1561–1574.

27 Zuccaro MV, *et al.* 2020. Allele-specific chromosome removal after Cas9 cleavage in human embryos. *Cell.* 183(6): 1650–1664.e15.

28 Akutsu SN, *et al.* 2022. iPSC reprogramming-mediated aneuploidy correction in autosomal trisomy syndromes. *PLoS One.* 17(3):e0264965.

29 Hirota T, *et al.* 2017. Fertile offspring from sterile sex chromosome trisomic mice. *Science.* 357(6354):932–935.

30 Truong MA, Cané-Gasull P, Lens SMA. 2023. Modeling specific aneuploidies: from karyotype manipulations to biological insights. *Chromosome Res.* 31(3):25.

31 Nahmad AD, *et al.* 2022. Frequent aneuploidy in primary human T cells after CRISPR-Cas9 cleavage. *Nat Biotechnol.* 40(12): 1807–1813.

32 Abdel-Hafiz HA, *et al.* 2023. Y chromosome loss in cancer drives growth by evasion of adaptive immunity. *Nature.* 619(7970): 624–631.

33 Girish V, *et al.* 2023. Oncogene-like addiction to aneuploidy in human cancers. *Science.* 381(6660):eadg4521.

34 Eleveld TF, *et al.* 2021. Engineering large-scale chromosomal deletions by CRISPR-Cas9. *Nucleic Acids Res.* 49(21):12007–12016.

35 Shih J, *et al.* 2023. Cancer aneuploidies are shaped primarily by effects on tumour fitness. *Nature.* 619(7971):793–800.

36 Truong MA, *et al.* 2023. A kinesin-based approach for inducing chromosome-specific mis-segregation in human cells. *EMBO J.* 42(10):e111559.

37 Tovini L, *et al.* 2023. Targeted assembly of ectopic kinetochores to induce chromosome-specific segmental aneuploidies. *EMBO J.* 42(10):e111587.

38 Bosco N, *et al.* 2023. KaryoCreate: a CRISPR-based technology to study chromosome-specific aneuploidy by targeting human centromeres. *Cell.* 186(9):1985–2001.e19.

39 Ma W, Liu Y, Ma H, Ren Z, Yan J. 2021. Cis-acting: a pattern of lncRNAs for gene regulation in induced pluripotent stem cells from patients with Down syndrome determined by integrative analysis of lncRNA and mRNA profiling data. *Exp Ther Med.* 22(1):701.

40 Wang Y, *et al.* 2021. The study of alternative splicing events in human induced pluripotent stem cells from a Down's syndrome patient. *Front Cell Dev Biol.* 9:661381.

41 Martinez JL, *et al.* 2024. Transcriptional consequences of trisomy 21 on neural induction. *Front Cell Neurosci.* 18:1341141.

42 Sarver DC, *et al.* 2023. Hypermetabolism in mice carrying a near-complete human chromosome 21. *Elife.* 12:e86023.

43 Alldred MJ, Martini AC, Patterson D, Hendrix J, Granholm AC. 2021. Aging with Down syndrome-where are we now and where are we going? *J Clin Med.* 10(20):4687.

44 Pal U, *et al.* 2021. The etiology of Down syndrome: maternal MCM9 polymorphisms increase risk of reduced recombination and nondisjunction of chromosome 21 during meiosis I within oocyte. *PLoS Genet.* 17(3):e1009462.

45 Nakagawa M, *et al.* 2014. A novel efficient feeder-free culture system for the derivation of human induced pluripotent stem cells. *Sci Rep.* 4:3594.

46 Miyazaki T, Isobe T, Nakatsuji N, Suemori H. 2017. Efficient adhesion culture of human pluripotent stem cells using laminin fragments in an uncoated manner. *Sci Rep.* 7:41165.

47 Linthorst J, *et al.* 2020. Extreme enrichment of VNTR-associated polymorphicity in human subtelomeres: genes with most VNTRs are predominantly expressed in the brain. *Transl Psychiatry.* 10(1):369.

48 Slaymaker IM, *et al.* 2016. Rationally engineered Cas9 nucleases with improved specificity. *Science.* 351(6268):84–88.

49 Bae S, Park J, Kim JS. 2014. Cas-OFFinder: a fast and versatile algorithm that searches for potential off-target sites of Cas9 RNA-guided endonucleases. *Bioinformatics.* 30(10):1473–1475.